The Computational Analysis of a Generic Hypersonic Store Separation

Ryan C. Savery[1,2]
University of Tennessee, Knoxville, TN 37996
Oak Ridge National Laboratory, Oak Ridge, TN 37831

James G. Coder[3]
The Pennsylvania State University, College Park, PA 16802

Many current hypersonic vehicles involve a main vehicle from which components separate during flight and presents simulation challenges such as shock-shock interactions, highly nonlinear interactions, and shock wave boundary layer interactions. These aerodynamic phenomena influence the attitude and trajectory of each object, which needs to be understood before large-scale experiments can be run. To gain a generic understanding of the process, high-fidelity Reynolds-averaged Navier-Stokes solutions are performed on a conical vehicle geometry passing through an oblique shock wave that is representative of different configurations and scenarios. Trajectory and applied forces are tracked and show the vehicle's dynamics are predominantly the result of differential flow incidence angles causing a strong shock; this leads to a large pressure increase over a fraction of the vehicle, which influences pitch. The vehicle appears to follow conventional stability theory with detached eddy simulation and small disturbances in initial attitude shown to have minimal influence on the scenario.

I. Introduction

Hypersonic vehicles fly at or above roughly Mach 5, which causes high aerodynamic and thermal loads arising from complex flow fields. These speeds are a necessity for space vehicles returning from orbit and beneficial to the modern warfighter for the ability to quickly and effectively deliver integrated or separated packages to a location. Many current hypersonic vehicles involve a main vehicle (i.e., a parent) with smaller components (i.e., a store or child) that separate during flight. These factors present physical simulation challenges like shock-shock interactions, shock wave boundary layer interactions (SBLIs), and other highly nonlinear interactions. These aerodynamic phenomena influence the attitude and trajectory of each object and needs to be understood before large-scale experiments can be conducted. The dynamics of an individual hypersonic vehicle have been studied extensively [1-3], whereas smaller payloads being separated from a larger vehicle as a topic of study has been relatively ignored in literature. This process of detaching a child vehicle from a parent vehicle is known as *store separation*.

Stores are often axisymmetric shapes that are statically stable in free flight. This means its attitude will restore with no control inputs if its angle of attack or sideslip are slightly perturbed [7]. Static stability is a product of the center of gravity's (CoG's) location relative to the neutral point (NP)—in other words, the point at which the aerodynamic moment coefficient does not change with pitch angle relative to the flow or angle of attack (AoA).

[1] Graduate Research Assistant, Mechanical, Aerospace and, Biomedical Engineering, Student, AIAA Member
[2] Research and Development Assistant, Enrichment Science and Engineering Division
[3] Associate Professor, Department of Aerospace Engineering, Associate Fellow AIAA

Generally, a statically stable vehicle has the CoG location forward of the NP, thereby providing a corrective force and returning the vehicle parallel to the external flow. The amount of correction can be characterized by the static stability margin, which is based on the distance of the NP from the CoG to the total vehicle length. To generically understand a vehicle's dynamics due to outside influences, it can be advantageous to separate the stability forces from the applied aerodynamic forces. This can be accomplished by collocating the CoG and NP, thereby eliminating stability forces and making the vehicle statically neutral. The aerodynamic forces (e.g., lift, drag, and side force) act through the center of pressure (CoP)—the average point at which the total surface pressure acts on the body. Depending on the geometry of the vehicle, the CoP can change with AoA, which is not desirable when attempting to decompose the applied forces. A vehicle with a static CoP location, collocated with the NP, should be chosen for this type of experiment. Notably, hypersonic vehicle stability and control properties have also been shown to potentially vary from lower speed vehicles in a few ways [5]: (1) The CoP changes relatively little with changes in AoA and altitude, (2) maximum lift to drag ratios are typically small in the 1–5 range and are nonlinear with AoA, and (3) stability margin is a less effective measure of true vehicle stability. Many of the differences are an effect of the strong shocks near surfaces and influence vehicles of all shapes.

Early store separation analysis efforts focused on subsonic aircraft and used a combination of flight and wind tunnel tests to understand the trajectory after release [4]. These tests showed the force of gravity to prevail over any aerodynamic force, preventing upward movement after release and negating the need for collision analysis. As speeds increased into the transonic, supersonic, and hypersonic regime, payload and vehicle configurations became more complex and the applied forces on the store were able to overcome the gravitational force. The store's attitude was determined by unbalanced forces and moments acting on the body caused by flow field features, including boundary layers, shear layers, shocks, and expansions along with the stability characteristics of the vehicle [5, 6]. Store carrying location played a major role in determining these factors and can be split into two categories: (1) external carry with the store carried underneath the wing or fuselage of the parent vehicle, and (2) internal carry, wherein the store is typically held within a closed cavity and opened before release.

Analyzing hypersonic vehicle configurations using wind tunnels and flight tests requires an abundance of infrastructure, time, energy, and funding. Although these methods are needed for flight vehicles, utilizing simulation tools like computational fluid dynamics (CFD) and six degree-of-freedom (6DoF) rigid body dynamics codes allow for more cost-effective testing while still capturing high-fidelity data. Beginning in the late 1970s and early 1980s, CFD methods could capture the flow field around a representative vehicle and store configuration of the time [8, 9], and have since advanced to provide more accurate and efficient codes capable of simulating the current hypersonic vehicles of interest. These combined CFD/6DoF simulations have been shown to be accurate in low-speed external store separation test campaigns [10]; nevertheless, public knowledge regarding hypersonic applications is minimal, which is a motivation for this study. Because the topic is of importance to national security, a generic approach is taken so that data can be published openly without compromising potentially sensitive information on realistic flight vehicles.

II. Approach

A. Geometry

To gain a better understanding of the fundamental dynamics, this study will focus on a CFD analysis of a simplified hypersonic store separation, wherein a store passes downward through an oblique shock wave. This scenario is representative of a few possible situations that can benefit from an understanding of the vehicle's applied force and moments along with its trajectory: (1) an internal store held within the parent vehicle's fuselage crossing the shock created off the leading edge of the parent; (2) an internal store ejected out of the rear of a parent vehicle and crossing the recompression shock; or (3) a vehicle separating a subset (e.g., a stage separation or a vehicle bifurcating).

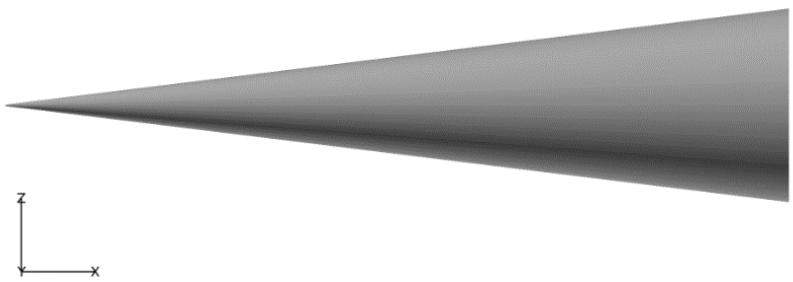

Figure 1. Generic Store Model

A flow field using a freestream Mach number of 7 and generic 20° oblique shock wave is used to eliminate the influence of any additional flow features created by the parent vehicle. A representative store was chosen that does not mimic any real-world geometry but could still provide useful data to the hypersonics field. A 7° half angle cone (Fig. 1) is used for its prior ubiquity in hypersonic fundamental work and has been shown by Ostapenko [11] to have a static CoP while varying AoA in free air. This signifies the CoP is collocated with the NP and potential movement is solely caused by outside influences. By placing the CoG at the CoP/NP location, the goal of disassociating stability forces from applied forces is accomplished as the vehicle should be statically neutral regardless of attitude.

The nondimensional model uses a length of 1 with a nose radius 0.1% of its length that meets tangentially with the conical section. To dimensionalize the store for calculating 6DoF trajectories, an experimental model from Hyslop et al. [12] was closely matched, resulting in the geometric and inertial properties, summarized in Table 1, that are nondimensionalized using the vehicle's length, free stream dynamic pressure, and static temperature of each run. The CoG was chosen to be 66.59% aft of the nose, which coincides with the CoP found from a static simulation discussed in subsequent sections.

Table 1: Representative Geometric and Inertial Properties

Length (mm)	250
Cone Half-Angle (◦)	7
Nose Radius (mm)	0.25
CoG (mm from nose)	166.48
Mass (g)	669.73
Moment of Inertia Ixx (kgm^2)	5×10^{-5}
Moment of Inertia Iyy (kgm^2)	2.15×10^{-3}
Moment of Inertia Izz (kgm^2)	2.15×10^{-3}

B. Numerical Methodology

All simulations were performed using the OVERFLOW 2.3e code developed and maintained by NASA [13]. It is a structured, overset, Reynolds-averaged Navier-Stokes (RANS) solver using a density-based, node-centered, finite-difference approach. OVERFLOW is capable of simulating 2D, axisymmetric, and 3D geometries; it supports 6DoF motion along with off-body grid adaptation. The HLLE++ flux scheme [14] is used for its ability to capture non-grid-aligned shocks with a fifth order spatial weighted essentially non-oscillatory (WENO5) reconstruction scheme [15]. Implicit solutions are handled by a symmetric successive over-relaxation (SSOR) method because it quickly converges and remains stable. The Spalart-Allmaras closure model (SA-neg-noft2) is used for turbulence and a second order backward differentiation formula (BDF2) with dual-time stepping sub-iterations advances time [16].

The overset grid systems were created by first using Pointwise to generate patches covering the surface of the vehicle [17]. Near-body volumetric grid generation was handled using the Chimera Grid Tools package and extended tangentially from the vehicle's surface so most of the flow features are captured in this region [18]. The near-body grid system, shown in Fig. 2, is placed within an off-body grid system that is either user-defined with the aforementioned grid-generation tools or automatically generated in OVERFLOW. The off-body grids contain a refinement region encapsulating the near-body grids with closely matched grid spacings, which extend one vehicle length behind the aft plane. Near-body grids and some refinement regions will track the vehicle's movement within the stationary off-body system with connection between grids handled using OVERFLOW's built-in domain connectivity function. Computational grids were constructed following the best practices, outlined by Spalart [19], in

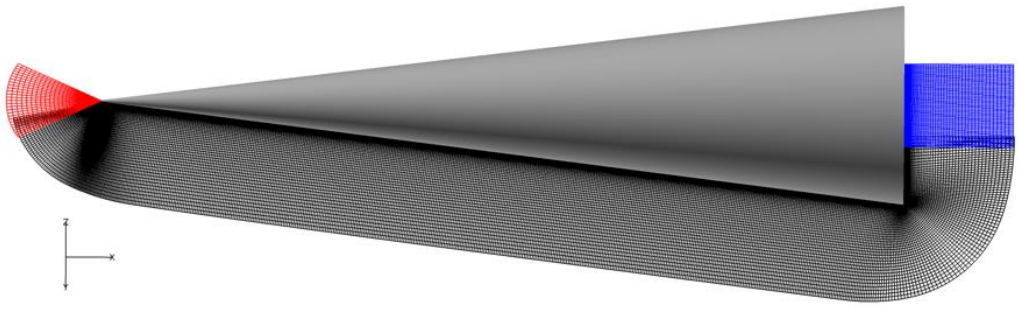

Figure 2. Near-Body Grid System 2D Slice

nondimensional space where the length of the vehicle is one unit. The viscous wall spacing used a y^+ value of 0.667 referenced from free stream conditions, and a global maximum stretching ratio of 1.15 was used to grow the grid.

C. Simulation Initialization

To form an oblique shock through the domain, the top boundary condition used a custom inflow condition with a state before and after the shock. The state in front of the shock mimics the freestream conditions with the downstream flow direction and properties calculated using oblique shock theory [20], thereby resulting in a 20° shock and 13.52° flow deflection angle. The upstream boundary used prescribed freestream conditions and the sides of the domain modeled used symmetry planes to continue the shock throughout. Symmetry planes can introduce nonphysical flow features into the domain where the vehicle's shock meets the boundary; however, these boundaries were extended such that interactions were sufficiently downstream to not impact the solution of interest. All other boundaries were set to Riemann characteristic outflow conditions.

Solutions were initialized by ramping the freestream Mach number and custom boundary condition using local time stepping to advect startup transients. A steady state solution formed when force and moment coefficients stabilized; time-accurate solutions were run thereafter. A maximum physical time step was chosen based on the time it takes a particle to flow roughly one grid unit on the surface of the vehicle in free air, then decreased based on stability considerations. Time-accurate solutions were performed using a maximum of 30 dual sub-iterations, wherein grid connectivity was updated every 100 iterations. The force and moment calculations were handled internally using the MIXSUR [21] module with OVERFLOW's 6DoF solver updating the trajectory and attitude every 10 iterations.

III. Results

A. Aerodynamic Properties

Before running complex simulations with multiple influential forces on the vehicle, it was advantageous to understand and validate the model in free flight against experiments and theory. To acquire a reference point, a simulation was run in Mach 7 free flow with a Reynolds number of 4.65×10^6 and a temperature of 83.34 °R. An adaptive off-body grid system was used, which tracked the vehicle orientation and contained approximately 15–18.5 million points depending on the attitude. The AoA was increased about its center (i.e., half of the vehicle's length) from 0–45° over 45 characteristic time steps with force and moment coefficients logged every 0.01°. The resulting force and moment, taken with respect to the vehicle's nose, coefficients along with lift-to-drag ratio are plotted in Fig. 3. This simulation was run at similar flow conditions to a free flight wind tunnel experiment of the same geometry performed by Hyslop et al. [12], which tested AoAs from −7° to 7°. When qualitatively comparing this simulation to their results in the same AoA range, good agreement in lift, drag, and pitching moment coefficients were observed; however, further quantitative validation against experiments is desired, which were not available at the time of writing.

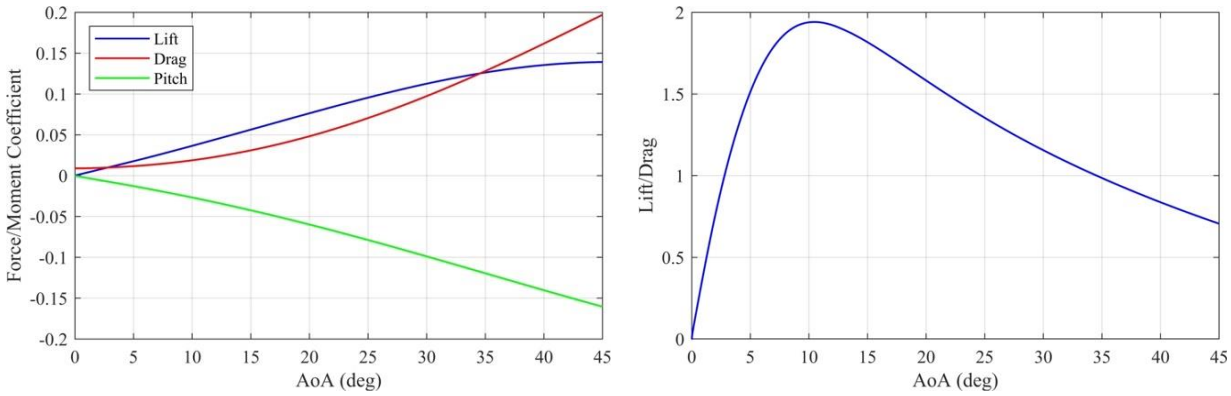

a) Aerodynamic Coefficients **b) Lift to Drag Ratio**

Figure 3. AoA Sweep Aerodynamic Coefficients

The CoP was calculated using Eq. 1, where x is the distance aft of the nose and p is the surface pressure, which is numerically integrated over the surface of the vehicle performed using FieldView [22]. This method was used for all CoP measurements herein unless otherwise stated.

$$CoP = \frac{\int x\, p(x)dx}{\int p(x)dx} \qquad \text{Eq. (1)}$$

To verify the CoP measurements, a modified Newtonian theory [23] code was developed using Matlab [24] where surfaces located in the wake were assumed to be a vacuum. The resulting analytical calculations give the CoP at 66.7% of the vehicle's length and CFD measurements vary from 66.3% to 66.6%. It should be noted that the CFD simulation had the CoP location move slightly forward with AoA, which could be the result of the added nose radius and flow separation at higher angles. The CoP location calculated by the empirical method, CFD simulation, and wind tunnel results from Hyslop et al. all give the location approximately 66.6% aft of the vehicle's nose regardless of AoA. This is promising validation of the method from 0° to 7° AoA and builds confidence in aerodynamic coefficient measurements outside of the experimental range. The store design has a low peak lift-to-drag ratio just shy of 2, thereby making it not particularly desirable for sustained flight because it would have little vertical and lateral controllability. Many stores, however, do not require control because they simply need to separate cleanly from the parent to accomplish their mission.

Considering the assumption of a collocated NP and CoP, the CFD CoP calculations should be unchanged with AoA which is not the case. The CoP moved forward on the vehicle, varying by 0.3% of the store's length, implying that the team's assumption is not entirely correct. This misassumption will result in a stabilizing force as the CoG is placed at the CoP, which is slightly forward of the true NP. The influence on the results is discussed in the following section.

B. Dynamic Simulation

Before running dynamic simulations, the custom inflow boundary condition needed to be validated. A single rectangular grid consisting of 147×101×67 points with clustering near the boundary and initial location of the shock was used. A larger 30° oblique shock—used to better resolve potential error sources—in Mach 7 free flow with a Reynolds number of 8.65×10^6 was arbitrarily chosen for the boundary condition. The flow properties across the shock in the middle of the domain are shown in Fig. 4 and closely match theory at the inlet and outlet. There are notable variances once crossing through the shock between $X/L = 0.1$ and $X/L = 0.5$ better shown by plotting a centerline cut of Mach number as in Fig. 5. Because the shock width is directly related to the grid spacing due to the numerical scheme capturing the shock over two grid points, these nonphysical features are believed to be caused by varying shock widths near the top boundary. To minimize this effect in subsequent simulations, care is taken to minimize varying grid spacing near the shock along with creating refinement regions that are shock aligned.

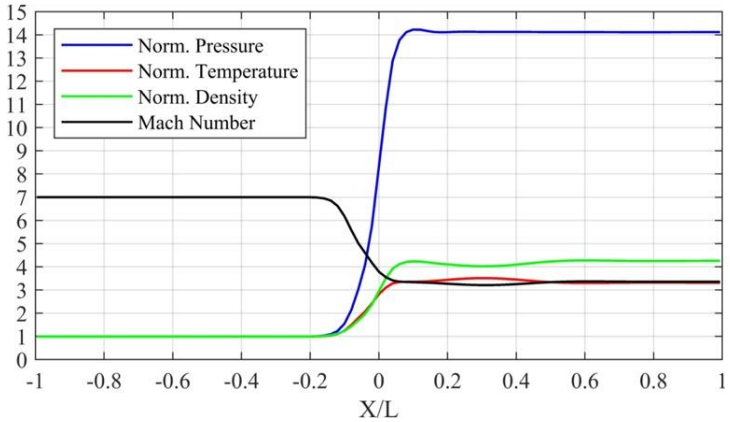

Figure 4. Flow Properties for Oblique Shock Boundary Condition

For the dynamic simulation, the entire grid system was user-defined with two off-body grid levels that tracked the vehicle, a refinement region at the top boundary, and a shock-aligned refinement region. The combined domain contains approximately 25×10^6 points and is pictured in Fig. 6 at a location mid-run. The vehicle is initially placed above the shock as to not create any interactions between the two. A downward velocity of 2.5 m/s was prescribed on the first time step to simulate the store having been influenced by gravity prior to the start. The built-in 6DoF dynamics solver was used to iterate location and attitude. The freestream inflow is at Mach 7 with a Reynolds number of 8.65×10^6 and static temperature of 288.2 K. A physical time step of 1×10^{-7} s was chosen based on numerical stability and corresponds to a nondimensional time step of approximately 0.001.

Figure 5. Mach Number Centerline Cut for Oblique Shock Boundary Condition

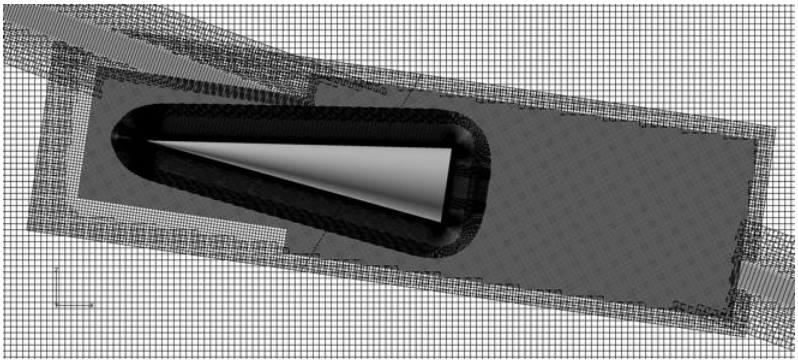

a) 2-D Centerline Slice

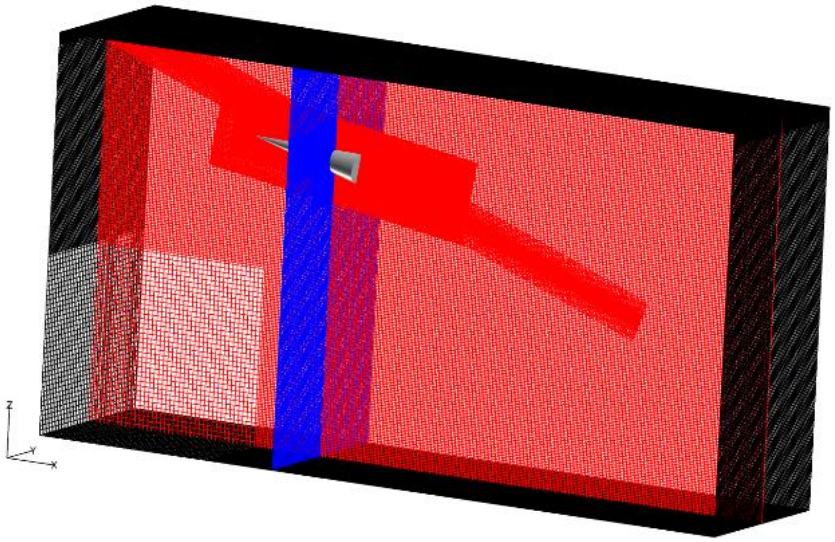

b) Full System

Figure 6. Dynamic Simulation Grid System

Instantaneous Mach number in the Y plane is plotted every 12 nondimensional time steps in Fig. 7, which shows the store moving downward while maintaining its attitude until encountering the shock and starting to pitch up continuously. This is confirmed by plotting the CoG trajectory, attitude, force coefficients, and moment (taken about the CoG) coefficients of the vehicle in Fig. 8. They show the downward motion dominating the velocity component, wherein the pitch slowly increases until encountering the shock. The pitch rate quickly increases, then decreases while crossing the shock, and continues linearly after this point. The location of peak moment occurs when the shock passes through the CoG if continued through the vehicle. After passing the shock, the vehicle is at an AoA in free air where the force and moments match those found in the free flight simulations.

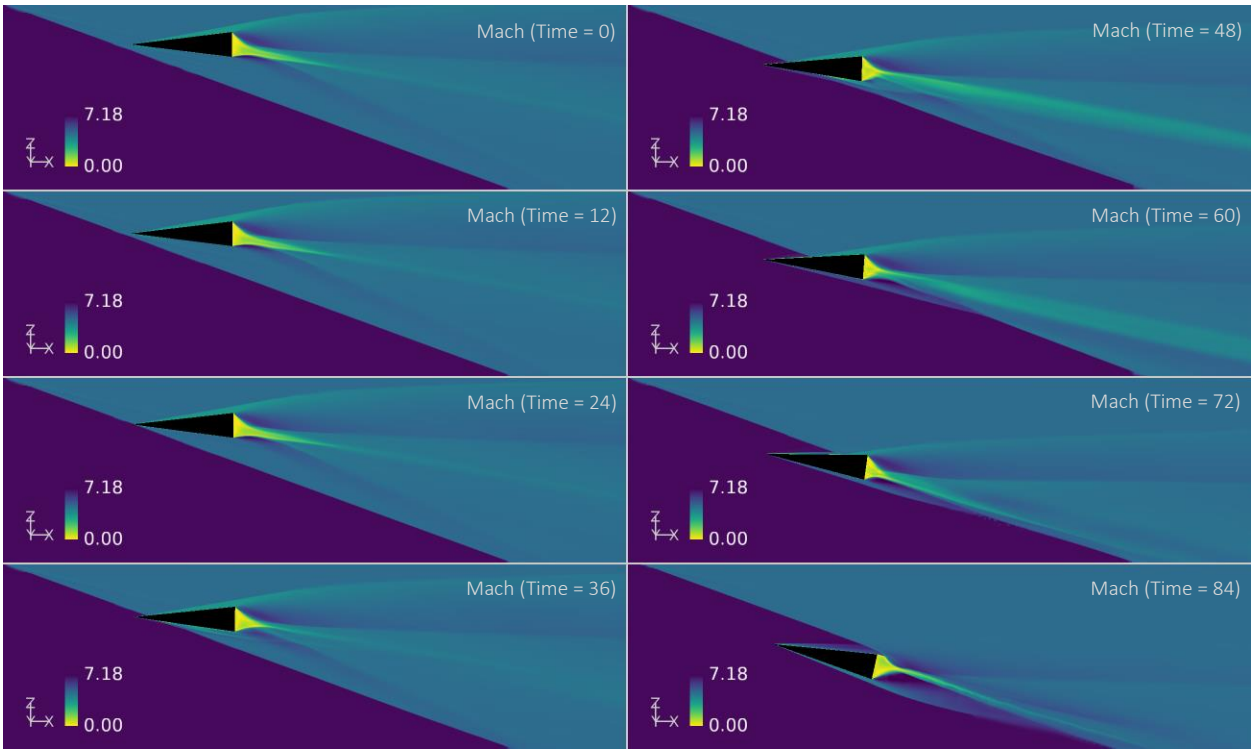

Figure 7. Sequence of Instantaneous Y-plane Mach Numbers in Nondimensional Time

Fig. 8d exhibits an initial positive moment (i.e., a restorative force turning the vehicle toward the incoming flow vector), thereby indicating some stability forces are present. The moment is small but shows that the CoG is slightly in front of the true aerodynamic center. This is also true after the vehicle passes through the shock shown by the negative moment increasing as the vehicle pitches up. This restorative moment has a maximum value of around 12.5% relative to the peak moment and is theorized to be caused by viscous and momentum effects pushing the calculated CoP slightly in front of the NP. It was shown post-run that moving the CoG location 0.1% aft would negate the initial moment variance. Due to the small force relative to the entirety of the run, it is thought to have little impact on the results.

The two flow incidence angles acting on the vehicle, along with a pitch change, implies the CoP location is not constant throughout the run. To test this theory, the CoP was calculated every 4 nondimensional time steps and plotted against the CoG in Fig. 9. It initially shows the CoP located at the CoG as expected, but as the vehicle starts to pass through the shock the CoP moves back along the vehicle's centerline gradually and peaks at 77.8% of the vehicle's length when measured from the nose. The CoP quickly returns to its original location as the rear clears the shock. The CoP movement directly coincides with the moment acting on the vehicle, which appears to be correlated with the area ratio on either side of the shock. The vehicle also becomes more stable during the interaction with the CoP moving aft and the peak pitching moment occurring when the shock passes through the CoG if continued through the body.

An instantaneous capture with the store mid crossing is given in Fig. 10 where normalized surface pressure is plotted using the viridis colormap with shocks, expansions, and boundary layers given in black and white by plotting density gradients solely for visualization. They confirm the large pressure increase on the surface behind the shock impact location and reflected shock. These facts show that the vehicle's dynamics are predominantly the result of differential flow incidence angles causing a stronger shock on the rear of the vehicle, creating a higher pressure behind the CoG and thus causing rotation.

Fig. 10 shows a complex SBLI and shock-shock interaction near the impact location. A boundary layer separation bubble is shown to align with an increase in surface pressure on the store in front of the shock impact location; however, the influence on the vehicle's dynamics should be small because the pressure contribution is minimal relative to that seen behind the shock. The interactions on the sides of the vehicle are complex and could affect vehicle designs in other ways, such as thermal and structural constraints not seen in free flight that must be addressed. Items that separate in this environment, especially those with high surface area-to-weight ratios like sensor covers, will experience complex flow fields, thus complicating trajectory calculations.

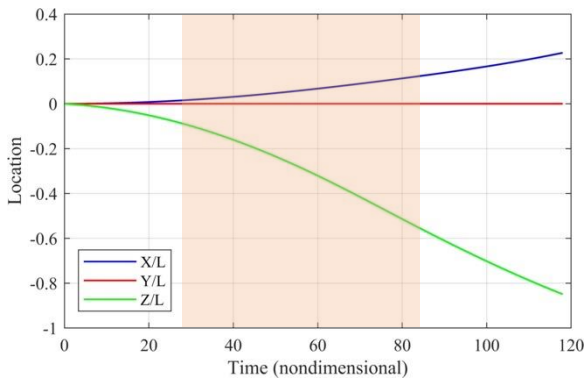

a) CoG Location

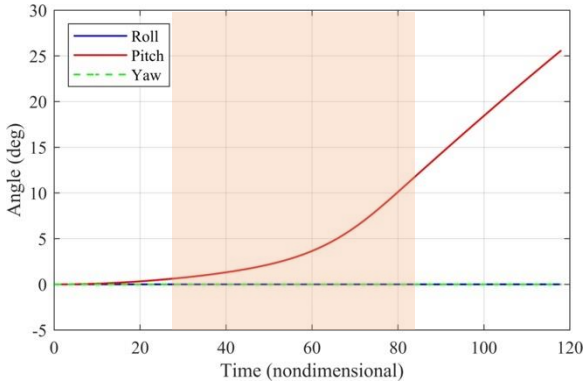

b) Attitude

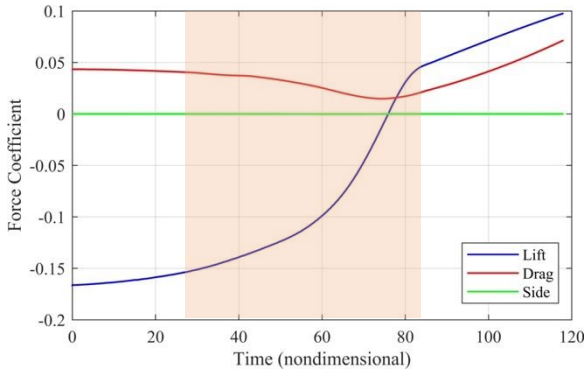

c) Force Coefficients

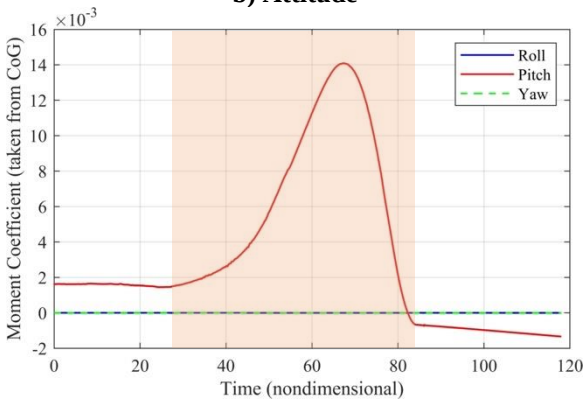

d) Moment Coefficients

Figure 8. Dynamic Simulation Trajectory and Aerodynamic Forces (Shock Encounter Highlighted)

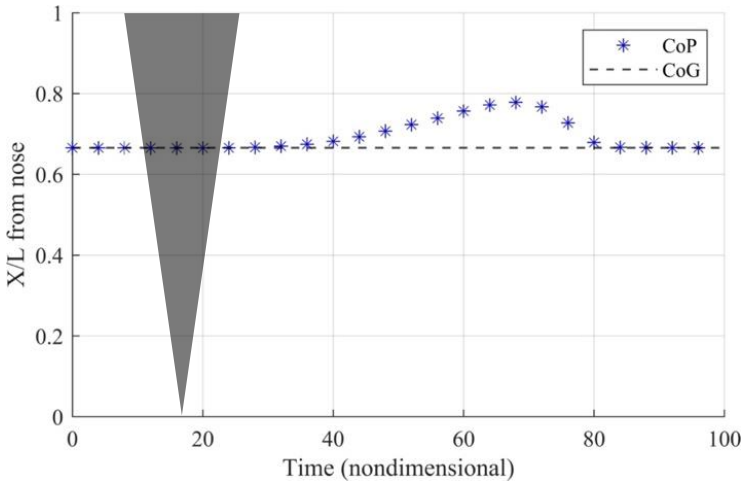

Figure 9. CoP Track for Dynamic Simulation

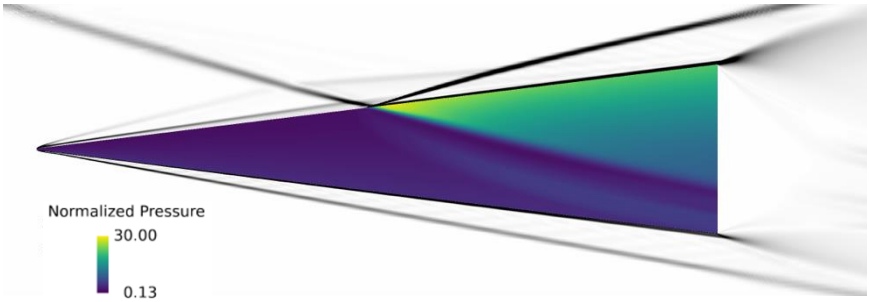

a) Side View

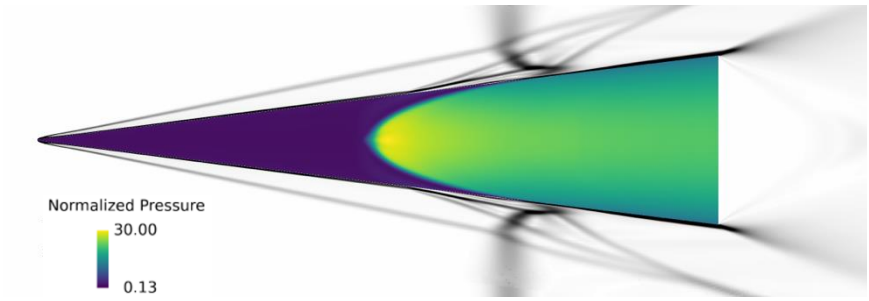

b) Top View

Figure 10. Instantaneous Normalized Surface Pressure Crossing Shock Relative to Flow Features

With this geometry, the time spent crossing the shock would have a large influence on the vehicle's attitude due to the solely positive moment applied. As the vehicle spends more time influenced by the shock, the integrated moment applied to the vehicle increases which can cause larger rotations. However, there is an equilibrium attitude between the two flow incidence angles approached because of the store being statically stable during the process. To minimize complications during a realistic store separation, a higher ejection force could be used to cross the shock faster. This could minimize the probability of upsetting the attitude and lower the corrective forces needed to return to stable flight. This would also decrease the possibility of a store with a low stability margin oscillating after being upset and recontacting the parent. An initial pitch down on ejection could allow the vehicle to turn back to level flight after crossing, but the ideal initial angle is geometry- and scenario-specific, thereby complicating the control problem. Notably, contrary to this test geometry's aerodynamic properties, many other vehicles' CoPs move forward with increasing AoA [5], which could negate the stabilizing effect of crossing the shock. Further studies using a geometry with this phenomenon are needed to understand the interaction between the two modes influencing CoP.

A key observation was that no upward movement was seen while crossing the shock. However, after passing, the vehicle is decelerating downwards due to the pitch up, and if not corrected, this would cause the vehicle to eventually lift. If not corrected with a larger static margin or active control, a collision could happen in a realistic scenario. Subsequent stability, control, and trajectory calculations once in free flight are needed to determine if separations are clean but are outside the scope of this study.

C. Uncertainty Analysis

Since there were no analogous studies at the time of writing, potential sources of uncertainty needed to be addressed. The free flight aerodynamic properties of the store were quantitively compared against theory and qualitatively against wind tunnel experiments within a range of AoAs and showed good agreement. This built confidence in the methods used, but other sources of uncertainty, such as grid refinement, numerical methods, and sensitivities, could impact the results. As such, these uncertainties were studied.

Regarding grid refinement, the grid spacing was chosen based on available computational hardware resources and is an order of magnitude larger than other hypersonic multi-body studies using similar techniques [25, 26], which were tested against flight experiments and exhibited good agreement. The grid systems used would be the most refined grid resolution if conducting a grid convergence study. For continued studies which might employ stochastic inputs, a smaller grid system would be desired to shorten run times. In this case, a grid refinement study should be conducted to determine the minimum points required to obtain a desired accuracy. Additionally, flow properties behind the shock at a location without the influence of the vehicle were probed and matched those values found from theory showing

little to no nonphysical intrusions from the boundary conditions. The shocks and wake region also appear to be appropriately captured with no visible steps in the solution.

The numerical schemes selected were well suited for hypersonic flow, but slow and stalled convergence was observed in the near-body grid along the sides of the vehicle during all simulations. Smaller shocks are revealed between the main attached shock and the vehicle's surface, which are not physical and appear to be the result of the non-shock aligned grid. Because the shock angles are not aligned with the near-body grids—ideally, the grid would be shock aligned but in dynamic simulations using Cartesian grids this is not possible because there are multiple different moving shocks—the attached shock will continue at a grid height normal to the surface until jumping to the next level to maintain its angle. These grid jumps appear to be at a similar location as the intermediary shocks and is a known issue with this family of numerical schemes.

The HLLE++ approximate Riemann solver has been shown by Tramel et al. to cause these variations in flow [14] at high sensitivity values (low DELTA values in OVERFLOW) of the multidimensional pressure switch used to locate shocks. All simulations in this study use a DELTA value of 1.5 to 3, which is much lower than those used by Tramel et al. to mitigate the effects. Larger DELTA values were attempted but caused instability in all solutions and for the residuals to stall. This is suspected to be caused by a bug in OVERFLOW 2.3e's SSOR method not using the proper HLLE++ inviscid flux. It used a suboptimal version of the HLLE+ flux which does not use a pressure switch to determine the switching function; instead, it uses a constant value of 1. (For an extended discussion on how the HLLE++ flux works, reference Tramel et al. [14].) The flux is formulated in a way that is effectively the HLLE flux. This adds excessive dissipation throughout the domain unlike HLLE++ which only uses HLLE near strong pressure gradients, such as shocks to maintain stability. To minimize stability issues during simulations, the pressure switch sensitivity value was lower than desired, thereby causing the steps in the main shock that led to the weak intermediary shocks. Fig. 11 shows the resulting surface pressure fluctuations (note the small range on the color bar) with the shocks plotted on the near-body grid using a shock capturing function for visualization. It shows extremely small fluctuations relative to the mean surface pressure and should have little effect on aerodynamic coefficient calculations as a result.

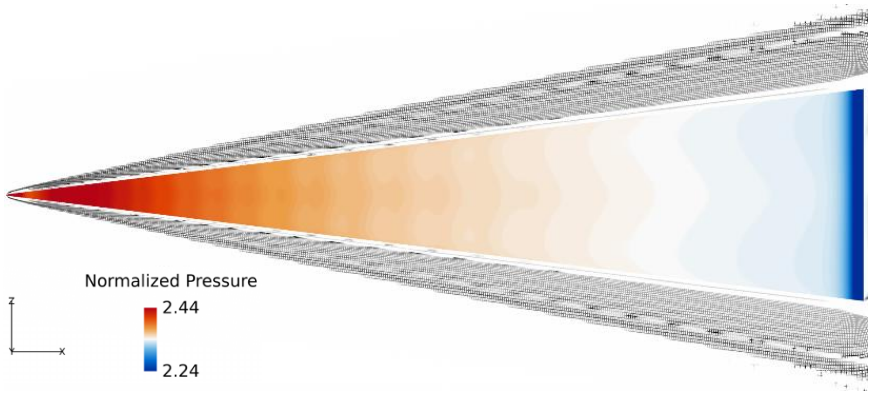

Figure 11. Normalized Surface Pressures in a Specified Range Relative to Shocks on the Near-Body Grid

To determine if the dynamic simulation had a sensitivity to disturbances in the initial attitude or 3D effects, an identical run was preformed wherein the vehicle would start with a yaw angle of −1°. The trajectory, attitude, and aerodynamic coefficients are plotted vs. the undisturbed run in Fig. 12. The store shows movement to the left throughout the simulation—which is a result of the side force applied due to the yaw angle, as expected. Minimal variances are seen in the X and Z directions, with any differences thought to be the result of increased drag acting on the vehicle from the additional yaw angle. Likewise, the pitching moment and resulting attitude are almost identical from run to run. As expected, the previously described residual stability moment influences yaw as it does pitch (i.e., increasing while passing through the shock); however, an unexpected roll moment was induced during this run. The cause for the roll moment is thought to be due to the top right of the store experiencing a marginally higher pressure than the top left, whereas the wake region below the store remains relatively unaffected which moves the CoP off the center line and induces roll. While small in this run, simulations that feature the store having a larger yaw angle or are nonaxisymmetric could amplify the roll moment and thereby rotate the lift vector to cause larger trajectory deviations. Further studies are needed to understand this effect. The findings from the sensitivity analysis indicate that this specific scenario is not significantly influenced by 3D effects resulting from disturbances in the initial attitude of the store.

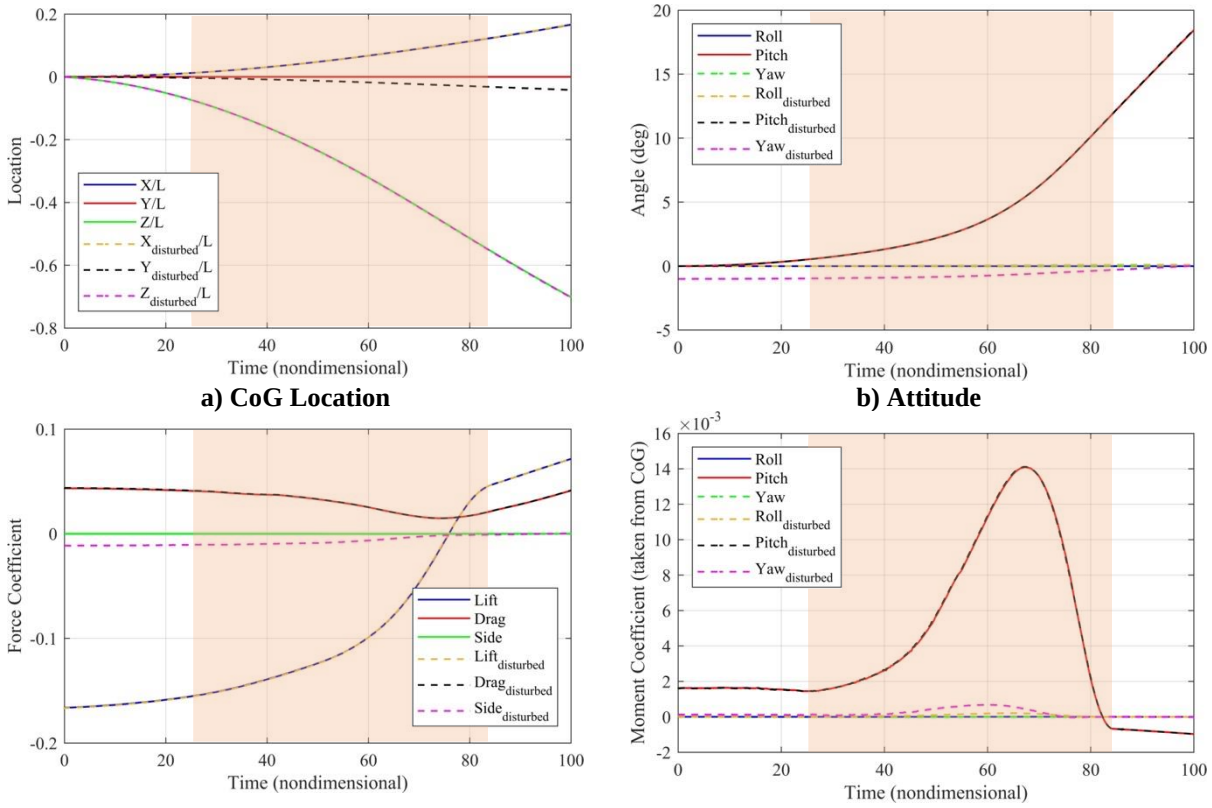

a) CoG Location **b) Attitude**

c) Force Coefficients **d) Moment Coefficients**

Figure 12. Stability Analysis Trajectory and Aerodynamic Forces (Shock Encounter Highlighted)

The use of hybrid RANS/large eddy simulation (LES), specifically delayed detached-eddy simulation (DDES), was tested to determine its impact on results when compared to RANS simulations. DDES is a slightly altered form of detached-eddy simulation (DES), wherein it uses RANS within the attached boundary layer and LES in the wake and separation regions [19]. With DES, careful grid construction must be done to accurately capture flow features. For this study, the original grid was constructed using the DES best practices outlined by Spalart [19]. Two simulations were run, in which the vehicle was held statically at the same location and attitude as the point of peak moment during the dynamic simulation. The store has a pitch up angle of 5.64° and is partially through the shock, as shown in Fig. 13. The simulations were run time accurate using Newton subiterations. The force and moment coefficients were allowed to stabilize beforehand. Results were then averaged over a span of 1,000 iterations to eliminate any variances due to oscillations in the coefficients; Notably, these oscillations were deemed negligible after the fact. Lift, drag, and pitching moment coefficients, which have been previously shown to dominate dynamics, are tabulated in Table 2 along with the CoP location. When comparing the two solution methods, RANS predicts slightly more lift and drag but with the CoP closer to the nose, which causes a smaller pitching moment. These values, however, are small; the largest difference in drag is 0.4507% and should have a negligible impact on the results of this study. The DDES simulation was also shown to have a 10%–15% increase in CPU time per iteration. These combined results show no need to expend additional computational cost for the increased fidelity of DDES; nevertheless, store separation simulations that have a lower grid resolution, larger wake, or more flow separation regions could still benefit from additional simulation capability.

Table 2: RANS vs DDES Aerodynamic Properties Comparison

	RANS	DDES	Diff. (%)
Lift Coefficient	-6.6636×10^{-2}	-6.6621×10^{-2}	0.2248
Drag Coefficient	1.7589×10^{-2}	1.7510×10^{-2}	0.4507
Pitch Moment Coefficient	1.4943×10^{-2}	1.4946×10^{-2}	0.0261
CoP (X/L from nose)	0.7790	0.7791	0.0951

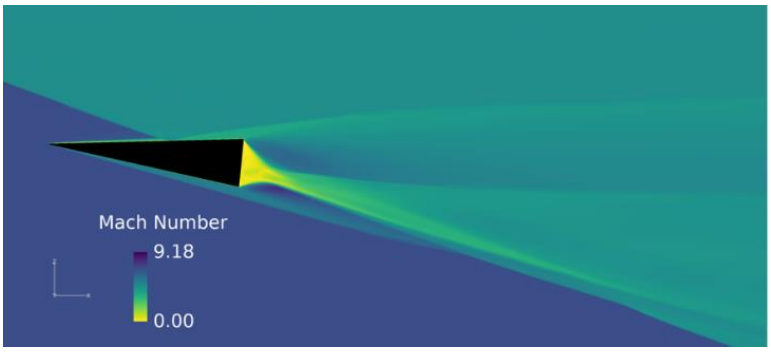

Figure 13. RANS Instantons Mach Number Showing DDES vs. RANS Comparison Location

IV. Conclusions

CFD was used to model a generic hypersonic store separation scenario to gain a fundamental understanding of associated physical phenomena, analyze current CFD analysis assumptions, and provide publicly available data on the subject. This experiment was specifically designed to be easily computationally or experimentally repeatable, allowing for future validation. A 7° cone was used for the store model because the applied forces and moments can easily be disassociated from those produced by the stability forces produced in free air. Two separate simulations were run with NASA's OVERFLOW 2.3e software using a free stream Mach number of 7. The store was placed in free air and swept from 0° to 45° AoA to confirm the aerodynamic properties against Newtonian theory and compare with wind tunnel experiments. It was then passed through a 20° oblique shock wave to generically simulate different separation scenarios with trajectory and attitude calculated using a 6DoF solver and aerodynamic coefficients were tracked. The store only pitches up while crossing the shock caused by the CoP moving aft because of a high-pressure region on the surface behind the oblique shock. The pitching moment gradually increases, peaks when the shock would pass through the CoG if allowed to continue through the body, then sharply decreases until returning to free air. There appears to be a direct relation between the ratio of surface on either side of the oblique shock, the CoP's location, and the moment applied to the store. Large separation regions were observed in front of the shock impact location caused by SBLIs. Results show that complex trajectories are possible in regions on the carrier vehicle containing SBLIs, such as near the empennage or engine cowling. Time spent crossing the shock is also shown to have a substantial impact on pitch angle, of which higher ejection velocities are desirable.

Because there are few available experimental studies on hypersonic store separation to validate the conclusions presented herein, assumptions were studied which could help identify and alleviate uncertainties. Grid refinement issues were identified and resolved using custom, high-resolution grids. Stalled convergence and stability issues were seen in the solution, theorized to be the result of an incomplete implicit solution method in OVERFLOW 2.3e. Higher fidelity DDESs were shown to have little impact on results, wherein aerodynamic coefficients and CoP location showed negligible differences. Likewise, no substantial sensitivities were observed when 3D effects were introduced using a small initial yaw angle.

References

[1] Thompson, M. O., "At the Edge of Space: The X-15 Flight Program", Washington, DC, and London: Smithsonian Institution Press, 1992.

[2] Isakeit, D., Watillon, P., Wilson, A., and Cazaux, C., "The Atmospheric Reentry Demonstrator", European Space Agency, 1998.

[3] McClinton, C., "X-43 - Scramjet Power Breaks the Hypersonic Barrier: Dryden Lectureship in Research for 2006," *44th AIAA Aerospace Sciences Meeting and Exhibit*, AIAA, Reno, Nevada, 2006. https://doi.org/10.2514/6.2006-1.

[4] Keen, K. S., Morgret, C. H., Langham, T. F., and Baker, W. B., "Trajectory Simulations Should Match Flight Tests and Other Lessons Learned in 30 Years of Store-Separation Analysis," *47th AIAA Aerospace Sciences Meeting Including the New Horizons Forum and Aerospace Exposition*, AIAA, Orlando, Florida, 2009. https://doi.org/10.2514/6.2009-99.

[5] Coleman, C. C., and Faruqi, F. A., "On Stability and Control of Hypersonic Vehicles," Tech. Rep. DSTO-TR-2358, Weapons Systems Division Defense Science and Technology Organization, 2009.

[6] Johnson, D., Thomas, R., and Manor, D., "Stability and Control Analysis of a Wave-Rider TSTO Second Stage," *10th AIAA/NAL-NASDA-ISAS International Space Planes and Hypersonic Systems and Technologies Conference*, AIAA, Kyoto, Japan, 2001, pp. 1–8. https://doi.org/10.2514/6.2001-1834.

[7] Pamadi, B. N., "Performance, Stability, Dynamics, and Control of Airplanes", AIAA, 2015.

[8] Moran, J., Tinoco, E. N., and Johnson, F. T., "User's Manual-Subsonic/Supersonic Advanced Panel Pilot Code," Tech. Rep. NASA CR-152047, Boeing Military Airplane Development, 1978.
[9] Steger, J. L., Dougherty, F. C., and Benek, J. A., "A Chimera Grid Scheme," 1983.
[10] Cenko, A., "Store Separation Lessons Learned During the Last 30 Years," *27th International Congress of the Aeronautical Sciences*, Naval Air Systems Command, Patuxent River, Maryland, 2010.
[11] Ostapenko, N. A., "On the Center of Pressure of Conical Bodies," (Translation) *Izvestiya Akademil Nauk SSSR, Mekhanika Zhidkosti i Gaza*, Vol. No. 1, Jan-Feb, 1980, pp. 99–104.
[12] Hyslop, A. M., McGilvray, M., and Doherty, L. J., "Free-Flight Aerodynamic Testing of a 7 Degree Half-Angle Cone," *AIAA SCITECH 2022 Forum*, AIAA, San Diego, California & Virtual, 2022. https://doi.org/10.2514/6.2022-1324.
[13] Nichols, R. H., and Buning, P. G., "User's Manual for OVERFLOW 2.3; Version 2.3d," Feb. 2021.
[14] Tramel, R., Nichols, R., and Buning, P., "Addition of Improved Shock-Capturing Schemes to OVERFLOW 2.1," *19th AIAA Computational Fluid Dynamics*, AIAA, San Antonio, Texas, 2009. https://doi.org/10.2514/6.2009-3988.
[15] Nichols, R. H., Tramel, R. W., and Buning, P. G., "Evaluation of Two High-Order Weighted Essentially Nonoscillatory Schemes," AIAA Journal, Vol. 46, No. 12, 2008, pp. 3090–3102. https://doi.org/10.2514/1.36849.
[16] Nichols, R., Tramel, R., and Buning, P., "Solver and Turbulence Model Upgrades to OVERFLOW 2 for Unsteady and High-Speed Applications," *24th AIAA Applied Aerodynamics Conference, American Institute of Aeronautics and Astronautics*, San Francisco, California, 2006. https://doi.org/10.2514/6.2006-2824.
[17] "Pointwise," Cadence Design Systems, 2023.
[18] Chan, W. M., Pandaya, S. A., Rogers, S. E., Jensen, J. C., Lee, H. C., Kao, D. L., Buning, P. G., Meakin, R. L., Boger, D. A., and Nash, S. M., "User's Manual for Chimera Grid Tools," 2018.
[19] Spalart, P. R., "Young-Person's Guide to Detached-Eddy Simulation Grids," Tech. Rep. NASA CR-2001-211032, Boeing Commercial Airplanes, Seattle, Washington, 2001.
[20] Anderson, J. D., "Modern Compressible Flow with Historical Perspective of Aeronautical and Aerospace Engineering." McGraw-Hill, New York, 1990.
[21] Chan, W. M., and Buning, P. G., "User's Manual for FOMOCO Utilities - Force and Moment Computation Tools for Overset Grids," 110408 Technical Memorandum 110408, NASA, 1996.
[22] "FieldView 21," Vela Software International, 2022.
[23] Heybey, W. H., "Newtonian Aerodynamics for General Body Shapes with Several Applications," Technical Memorandum X-53391, Space Flight Center, Huntsville, Alabama, 1966.
[24] "MATLAB R2018b," The MathWorks Inc., 2018.
[25] Buning, P. G., Gomez, R. J., and Scallion, W. I., "CFD Approaches for Simulation of Wing-Body Stage Separation," *22nd Applied Aerodynamics Conference and Exhibit*, AIAA, Providence, Rhode Island, 2004. https://doi.org/10.2514/6.2004-4838.
[26] Buning, P. G., Wong, T., Dilley, A. D., and Pao, J. L., "Computational Fluid Dynamics Prediction of Hyper-X Stage Separation Aerodynamics," Journal of Spacecraft and Rockets, Vol. 38, No. 6, 2001, pp. 820–827. https://doi.org/10.2514/2.3771.